Proceedings of Science and Mathematics
Faculty of science, universiti teknologi malaysia
https://science.utm.my/procscimath/
Volume 27 (2024) 35-48

Two-stages of Fouling Characterization in Industrial Textile Wastewater Removal via *Neolamarckia cadamba* Nanofibrillated Filter Paper Coupled to Crossflow Filtration System

Siti Solehah Ahmad Norrahma[a*], Nor Hazren Abdul Hamid[b], Latifah Jasmani[c], Nur Hanis Hayati Hairom[d]
[a]Nanotechnology Laboratory, Forest Products Division, Forest Research Institute Malaysia (FRIM), 52109 Kepong, Selangor, Malaysia
[b]Faculty of Engineering Technology, Universiti Tun Hussein Onn Malaysia, Pagoh Higher Education Hub, KM 1, Jalan Panchor, 84600 Muar, Johor, Malaysia
[c]Wood Chemistry and Non-Wood Utilization Program, Forest Products Division, Forest Research Institute Malaysia (FRIM), 52109 Kepong, Selangor, Malaysia
[d]Microelectronic and Nanotechnology-Shamsuddin Research Centre (MiNT-SRC), Faculty of Electrical and Electronic Engineering, Universiti Tun Hussein Onn Malaysia, 86400 Parit Raja, Batu Pahat, Johor, Malaysia
*Corresponding author: sitisolehah@frim.gov.my

Abstract
This study investigates the application of Weisner and Aptel's pore blocking models to assess the fouling mechanisms involved in treating industrial textile wastewater effluent using nanofibrillated cellulose (NFC) filter paper. By employing empirical models that depict the decline in permeate flux in a crossflow filtration system, the research aimed to identify fouling phenomena across various cellulose dosage ratios. NFC filter paper was fabricated from *Neolamarckia cadamba* and combined with bleached pulp in ratios of 50:50, 60:40, 70:30, 80:20, and 90:10. A comprehensive analysis of fouling behaviour was conducted to understand the removal efficiency of wastewater effluent. The study explored different blocking mechanisms, including cake formation, complete blocking, intermediate blocking, and standard blocking. Results demonstrated that the interaction between NFC filter paper and wastewater effluent led to distinct blocking mechanisms, analyzed over a two-stage with 2-hours operational period. The decline in flux was mainly attributed to the increased nanocellulose content, favouring a cake layer's formation. The findings suggest that cake formation predominantly governs the removal process, underscoring the effectiveness of NFC filter paper in achieving high colour removal and optimum normalized flux performance.
Keywords: Blocking filtration laws; textile wastewater; nanocellulose; NFC filter paper; Kelempayan

Introduction

The textile industry utilizes approximately 10,000 different dyes, as noted by Amin & Nizam (2016) (Amin & Nizam, 2016). The presence of carcinogenic compounds in untreated textile wastewater poses significant health risks to both humans and animals. Various essential processes have been developed to address this issue to remove colour from wastewater solutions. These treatments include the use of innovative nanomaterials in photocatalytic reactors, advanced oxidation processes (AOP), electrocoagulation, and the implementation of nanofiltration membrane technology (Samsami *et al.*, 2020). Numerous studies have underscored the effective application of nanofiltration membrane technology across diverse wastewater treatment scenarios, highlighting its potential to improve industrial textile wastewater management (Desa *et al.*, 2019; Hairom *et al.*, 2015; Saeed *et al.*, 2015; Sidik *et al.*, 2020).

Recent studies have highlighted the considerable promise of nanocellulose-based materials as an eco-friendly technology for effectively removing various pollutants in wastewater treatment due to the extensive surface area, strong binding and adsorption capabilities, and robust surface structure properties (Norrahma *et al.*, 2023). Nanocellulose, which is obtained through the modification or extraction of native cellulose, exists as a renewable resource found in nanoscale forms in plants,

animals, and microorganisms (Olaiya *et al.*, 2022). Collaborating with the Forest Research Institute Malaysia (FRIM), the research began by sourcing materials from Malaysian plantation forest species, specifically *Neolamarckia cadamba*, or commonly known as the Kelempayan tree. Cellulase enzymatic pre-treatment was employed to extract NFC and produce filter paper (Norrahma *et al.*, 2023). Recent investigations have focused on the compatibility and potential of NFC filter paper as an innovative nanotechnology for wastewater treatment, particularly in decolorizing industrial textile wastewater effluent using a crossflow filtration system.

Fouling presents a major challenge in membrane technology, affecting processes like ultrafiltration (UF), microfiltration (MF), nanofiltration (NF), and reverse osmosis (RO). It occurs when unwanted molecules from the feed accumulate on the membrane surface or within its pores, which can significantly reduce the efficiency and lifespan of the filtration process (Tanudjaja *et al.*, 2022). These fouling substances can include dissolved particles, partially soluble organic and inorganic macromolecules, and biological microorganisms. The type and extent of fouling depend on the location of the fouling within the membrane structure and the membrane's properties. Internal fouling is more common in UF and MF due to larger pore sizes and lower operating pressures. In contrast, surface fouling is typical in NF and RO systems because of their dense, semi-permeable membranes and higher pressures. To address fouling effectively, it is crucial to employ customized pre-treatment, cleaning methods, and membrane modifications (Alsawaftah *et al.*, 2021). Fouling in membrane processes can be detected by monitoring changes in permeate flux or transmembrane pressure (TMP) over time. A continuous decline in permeate flux at constant pressure or a gradual increase in TMP at a constant flux often signals fouling onset, hindering membrane performance (Marshall *et al.*, 1993). By closely observing these indicators, operators can detect fouling early and take corrective measures to ensure the optimal functioning of UF, MF, NF, and RO membrane systems (Ma & Chew, 2022; Nabi *et al.*, 2023). Through an understanding of fouling types and causes, and by implementing a combination of pre-treatment, membrane modifications, operational adjustments, and effective cleaning protocols, the negative impact of fouling can be minimized, leading to enhanced performance and longer lifespan of membrane filtration systems (Shen *et al.*, 2023).

$$\frac{d^2t}{dV_2} = K \times \left(\frac{dt}{dV}\right)n \qquad \textbf{(1)}$$

Blocking filtration laws were utilized to describe flux decline and fouling analysis, originally introduced by Hermans and Bredée in 1936 and later modified by Hermia in 1985 (Iritani & Katagiri, 2016). The model encompasses four distinct mechanisms: complete blocking, intermediate blocking, standard blocking, and cake formation. The blocking filtration laws can be determined using the equation presented in **Equation 1**, where V represents the volume of permeate at time t, and K is a coefficient dependent on flow rate and solution variables. Additionally, Wiesner and Aptel modified the model in 1996, as depicted in **Figure 1 (a)** and **(b)**, which illustrate two stages of blocking mechanisms represented by two different slopes (Wiesner & Aptel, 1996). In this model, the term K1 refers to the transfer of cake-forming components to the membrane. At the same time, K2 indicates the relative importance of back-transport mechanisms in removing materials from the membrane surface. According to Desa *et al.* (2019), the model verification is based on three principles: membrane resistance, pressure drops, and specific cake resistance that remains constant over time. The experimental results comprehensively explained how flux decline was evaluated in the present study.

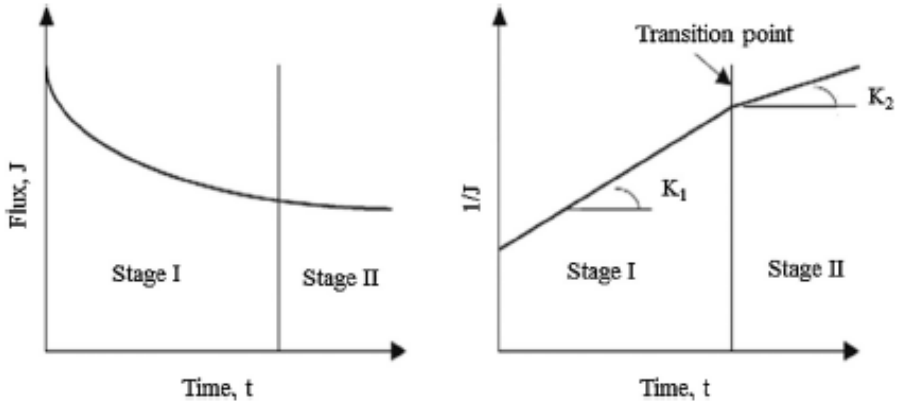

Figure 1 Membrane fouling mechanism formation (Wiesner & Aptel, 1996).

Complete blocking

Complete blocking is a type of surface fouling where foulant molecules accumulate on the membrane surface, fully obstructing the pores without forming layers on top of each other. In this mechanism, the deposited foulants block the pores entirely, preventing further passage of the feed solution through those blocked pores. This phenomenon occurs when the foulant molecules exceed the membrane's pores. The equation can be linearized to evaluate the linear relationship between permeate flux and contact time. In the case of complete blocking, with n=2, the equation is reformulated as shown in Equation 2. Figure 2 illustrates the linearized version of the complete blocking equation, where a plot of 1/J against time (t) should result in a straight line. The slope of this line is denoted as K, while the intercept corresponds to the initial flux or a term related to initial conditions. This model offers a clear approach to determining whether complete blocking is the primary fouling mechanism. The experimental validation, which reveals a linear relationship, confirms that flux decreases over time as resistance increases due to pore obstruction by foulants. Understanding this mechanism is essential for developing strategies to control fouling, optimize membrane performance, and extend the lifespan of filtration systems (Fernández *et al.*, 2011; Iritani & Katagiri, 2016).

$$-\ln\frac{J_0}{J} - 1 = Kt \tag{2}$$

where J_0 is the initial permeate flux (m/s), J is the permeate flux (m/s), K is the coefficient based on the flow rate and solution variables and t is permeate time.

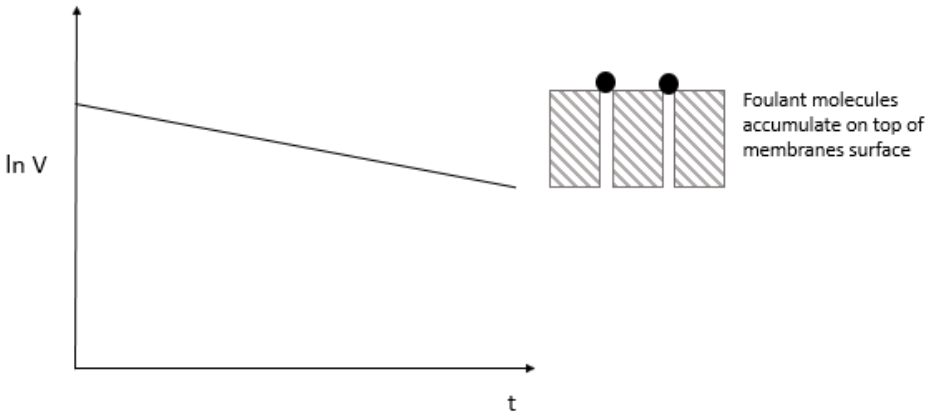

Figure 2 Complete blocking linear graph and mechanism illustration.

Standard blocking

Standard blocking occurs when foulant molecules accumulate and adhere to the membrane pores' internal walls, reducing the cross-sectional area and diameter of the pores as particles are retained. This blocking mechanism is relevant when the membrane's pore size exceeds the size of the foulant particles. The equation can be linearized to evaluate the relationship between permeate flux and time. In the case of standard blocking, with n=1.5, the equation is transformed as shown in Equation 3. Understanding the standard blocking model is crucial for grasping the impact of internal pore fouling on membrane filtration. By linearizing Hermia's equation and plotting $1/J^{2/3}$ against time, this model provides a framework to determine whether standard blocking is the dominant fouling mechanism. The experimental validation, which shows a linear relationship, confirms that permeate flux decreases over time as resistance increases due to internal pore fouling, as illustrated in Figure 3. This insight is essential for developing strategies to control fouling, optimize membrane performance, and prolong the operational life of filtration systems (Fernández *et al.*, 2011; Iritani & Katagiri, 2016).

$$\frac{\sqrt{J_0}}{J} - 1 = Kt \quad \textbf{(3)}$$

where J_0 is the initial permeate flux (m/s), J is the permeate flux (m/s), K is the coefficient based on the flow rate and solution variables and t is permeate time.

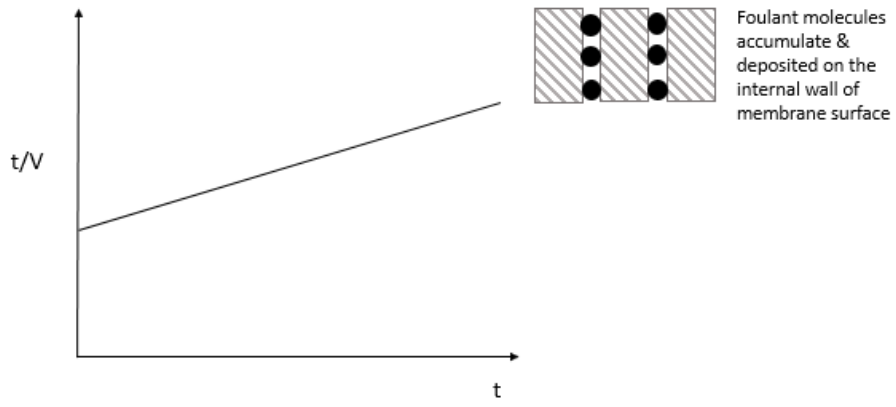

Figure 3 Standard blocking linear graph and mechanism illustration.

Intermediate blocking

Intermediate blocking is similar to complete blocking, with the key difference being that foulant particles deposit on the membrane surface and stack on each other or on areas of the membrane that have not yet been fouled. This phenomenon occurs when the foulant particles are larger than the membrane pores. The equation can be linearized to examine the relationship between permeate flux and permeate volume. With n=1, the equation is transformed for intermediate blocking, as outlined in Equation 4. The intermediate blocking model is crucial for understanding the impact of foulant particle stacking on membrane filtration. By linearizing Hermia's equation and plotting ln V (or 1/J) against time, as depicted in Figure 4, this model helps determine whether intermediate blocking is the primary fouling mechanism. A linear relationship in this context suggests intermediate blocking, where permeate flux declines as permeate volume increases due to the growing resistance from foulant deposition. The experimental validation, which demonstrates a linear relationship, confirms that permeate flux decreases with increasing permeate volume as resistance builds up, resulting from both pore blockage and the formation of a surface layer. This understanding is vital for developing effective strategies to mitigate fouling, enhance membrane performance, and extend the lifespan of filtration systems (Fernández *et al.*, 2011).

$$\frac{J_0}{J} - 1 = Kt \quad \textbf{(4)}$$

where J_0 is the initial permeate flux (m/s), J is the permeate flux (m/s), K is the coefficient based on the flow rate and solution variables and t is permeate time.

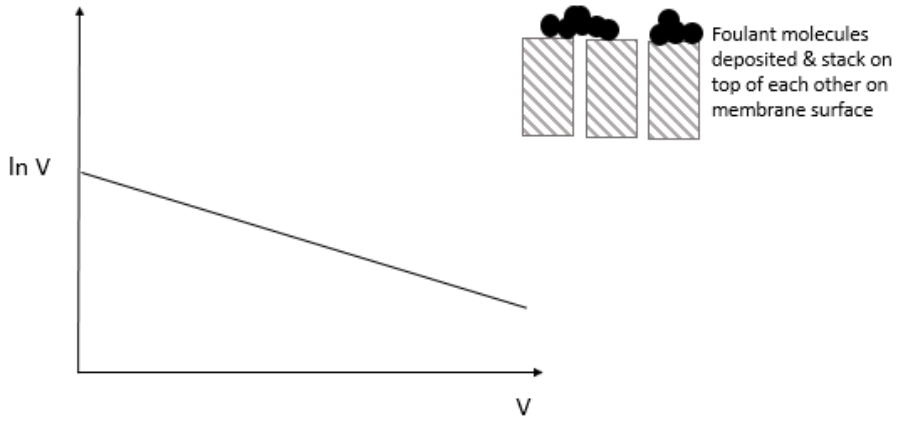

Figure 4 Intermediate blocking linear graph and mechanism illustration.

Cake layer formation

Cake formation occurs when foulant molecules accumulate and fully cover the membrane surface, leading to particles' stacking and forming a dense, thick layer. This phenomenon is common when foulant particles are much larger than the membrane pores, resulting in a cake layer that significantly increases flow resistance. The equation can be linearized to examine the relationship between permeate flux and permeate volume. The simplified equation is provided in Equation 5. The experimental flux data is plotted as V (permeate volume) against time (t) to validate the cake formation model. A linear relationship in this plot supports the cake formation assumption, showing that as the cake layer thickens, the permeate flux decreases due to increased resistance. Figure 5 illustrates the linear relationship between experimental data and permeate volume, indicating that as the mass transfer resistance rises with the cake layer's growth, the permeate volume decreases linearly over time. This confirms the applicability of the cake formation model with n=0. This understanding is crucial for developing strategies to control fouling, optimize membrane performance, and prolong the lifespan of filtration systems (Fernández *et al.*, 2011; Ho & Zydney, 2000; Iritani & Katagiri, 2016)

$$\left(\frac{J_0}{J}\right) - 1 = Kt \quad \textbf{(5)}$$

where J_0 is the initial permeate flux (m/s), J is the permeate flux (m/s), K is the coefficient based on the flow rate and solution variables and t is permeate time.

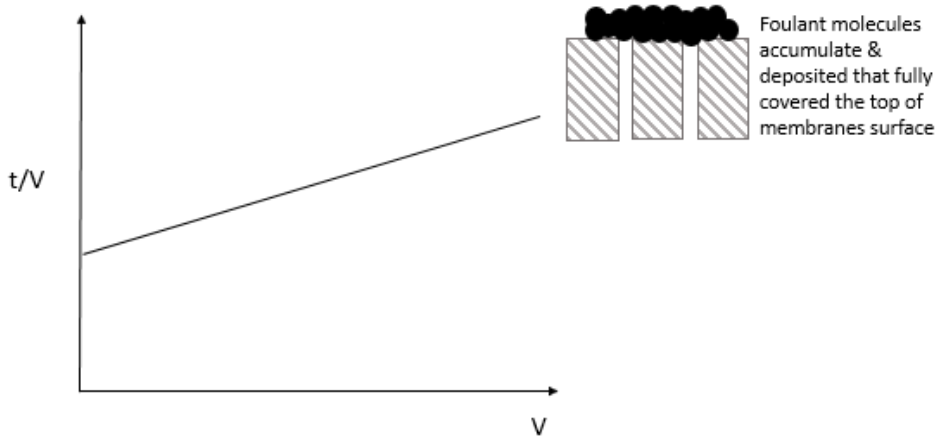

Figure 5 Cake layer formation linear graph and mechanism illustration.

This research delivers a thorough analysis of fouling mechanisms within a crossflow filtration system, employing varying dosages of NFC filter paper to treat industrial textile wastewater effluent. The study clarifies the dynamics of flux decline and the associated fouling mechanisms by utilizing Hermia's blocking filtration laws. This knowledge is essential for optimizing filtration procedures, ensuring effective effluent treatment, and extending the operational life of the membrane (Hermia, 1985). The findings offer deeper insights into how foulant molecules accumulate or become trapped on the filter paper surface, impacting colour removal efficiency. Consequently, this approach provided critical data and insights for addressing fouling challenges. With a more precise understanding of these fouling mechanisms and their effects on membrane performance, future strategies can be formulated to enhance the filtration process.

Materials and methods

Materials

The feed solution used for the filtration process was a textile wastewater sample originating from a textile factory in Johor, Malaysia, which conducts knitting, dyeing, finishing, and printing processes. This batch of textile wastewater was dark reddish at room temperature. The sample was collected in an air-tight container and stored in a chiller at 4 ◦C for preservation purposes before use. Distilled water was used prior to dissolving the required substances. The effluent colour intensity was measured by utilizing a Hitachi U-3900H UV-Vis Spectrophotometer.

This study examined four different combination dosage ratios of nanofibrillated cellulose (NFC) with the bleached pulp filter paper, which were 50:50, 60:40, 70:30, and 80:20. The NFC was synthesized from *Neolamarckia cadamba*, following the kraft pulping and bleaching process as first reported by Latifah *et al.*, (Latifah *et al.*, 2020). The enzymatic pre-treatment involved the use of *Aspergillus niger* cellulase enzyme to refine the material further. The process utilized 2300 g of bleached pulp from the previous stage, 8.2 g of sodium acetate ($C_2H_3NaO_2$), 2.5 g of cellulase enzyme, and 2.0 L of distilled water. The enzymatic reaction was carried out under controlled conditions—at 28 °C with a stirring rate of 80 rpm for 72 hours. Afterward, the sample was immersed in hot water to deactivate the enzyme. The subsequent preparation and fabrication procedures were based on the method developed by Norrahma *et al.*, (Norrahma *et al.*, 2023). Fig. 6 displayed the NFC filter paper fabricated for use in this study.

Fig. 6 NFC filter paper fabricated from *Neolamarckia cadamba*

Experimental design and set-up

The crossflow filtration system was deliberately selected due to its ability to manage the necessary pressure and flow conditions, making it ideal for conducting comprehensive permeability studies. Water permeability testing involved circulating distilled water through the NFC filter paper at a pressure of 3 bars for 30 minutes during the wetting phase. This step was essential to avoid repeated compaction and ensure the NFC filter paper was thoroughly wetted, which helped maintain consistency and accuracy in the permeability measurements. Figure 7 provides a schematic representation of the crossflow filtration system employed in this study. The system featured a 2-liter reactor tank designed to hold the feed solution, connected to a separation unit—the Sterlitech™ HP4750 crossflow filtration system. The filtration studies were conducted using the NFC filter paper with an effective filtration area of 20.60 cm². The study aimed to generate precise and reliable data on the water permeability of the NFC filter paper by utilizing a crossflow filtration system with a defined effective filtration area and ensuring thorough wetting. This setup is critical for understanding the filtration properties and potential applications of NFC filter paper in various filtration processes.

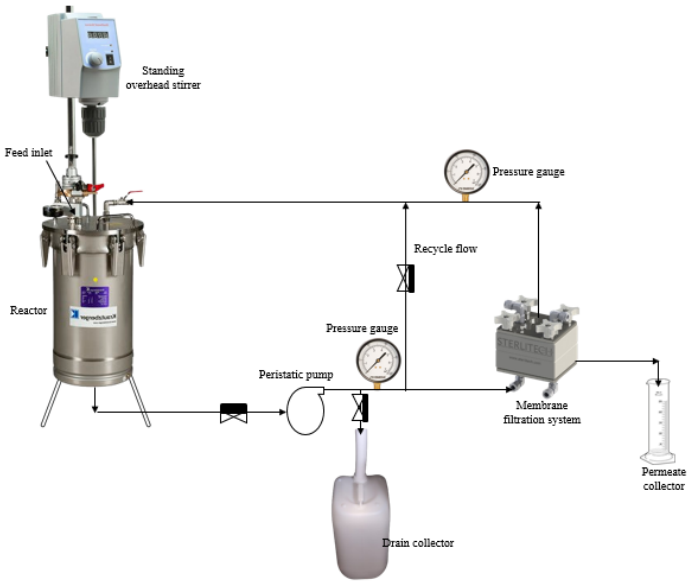

Figure 7 Schematic diagram of crossflow filtration system.

The permeation studies further examined the permeability procedure by focusing on the effective filtration area of the NFC filter paper, ensuring precise measurement and control throughout the filtration process. Building on the work of Norrahma *et al.*, (2023), a similar methodology was adopted, but with variations in the NFC filter papers, each featuring different combination ratios of NFC and bleached pulp. The specific ratios tested were 50:50, 60:40, 70:30, and 80:20. These filter papers were integrated into the filtration system to evaluate their performance under different conditions. Industrial textile wastewater effluent was circulated through the system with a pH of 6.5 and at 100% concentration.

Permeate flux readings were taken every 5 minutes for 2 hours. This data allowed for assessing filtration performance and the impact of varying mixing ratios on fouling behaviour. By regularly monitoring the permeate flux, the study provided insights into fouling mechanisms and filtration efficiency for different filter paper compositions. This method is crucial for optimizing filter materials to enhance dye removal efficiency and improve resistance to fouling.

By calculating the volume of permeate (V) per unit area (A) per unit time (t), the pure water flux (J_0) for each NFC filter paper sample can be determined. The pure water flux is a key parameter that indicates the membrane's permeability under test conditions. The specific equation used to calculate J_0 as stated in Equation 6.

$$J_0 = \frac{V}{At} \quad \textbf{(6)}$$

By calculating the instantaneous permeate flux (J) at different time intervals, the performance of the NFC filter paper can be monitored over the duration of the experiment. This helps in understanding how the flux changes with time, indicating the onset and progression of fouling.

$$J = \frac{V_2 - V_1}{A(t_2 - t_1)} \quad \textbf{(7)}$$

Blocking filtration laws

The fouling mechanism for NFC filter paper at various dosage ratios was identified using the Wiesner and Aptel equations. MATLAB R2023b was the main software employed to compute and plot the y-axis and x-axis according to the blocking filtration rules against time data. The fitted parameter constant (K) and the model fitness level (R^2) were used to elucidate the fouling mechanism.

Results and discussion

Compatibility assessment with crossflow filtration system

A good membrane's most crucial quality is maintaining consistent water permeability with less than 1% change in permeance over an hour following membrane compaction. However, most nanocellulose membranes face challenges with low permeability performance despite having high rejection capacities. This study aimed to analyze the compatibility of NFC filter paper with a crossflow filtration system in the absence of pollutants. The water permeability of NFC filter paper was tested using distilled water at various pressures. The results are plotted in Fig. 8, which shows the flow rate of distilled water against pressure for each NFC filter paper composition. The R^2 value greater than 0.90 was observed for all NFC filter paper compositions, suggesting a strong linear relationship and high consistency in permeability measurements. The water permeability at 3 bars of pressure for NFC filter paper with different cellulose dosages of 50:50, 60:40, 70:30 and 80:20 was 674.73, 34.59, 20.00 and 150.19 $Lm^{-2}hr^{-1}$, respectively. It should be noted that the cellulose dosage of 90:10 was incompatible in this study, where the samples ruptured during the examination at 1 bar pressure of distilled water through the crossflow filtration system.

To ensure compatibility and performance, maintaining density with high porosity while achieving high permeance is crucial for producing quality nanopaper (Yousefi *et al.*, 2021). This study revealed that NFC filter paper performed well within the crossflow filtration system at cellulose dosages of 50:50, 60:40, 70:30, and 80:20. This effectiveness can be attributed to the looser fibril networks within the NFC filter paper, which created a more porous structure with a greater void volume. This configuration increased the resistance to water molecules attempting to penetrate the paper surface but still allowed for sufficient permeability. The inclusion of bleached pulp was critical in this balance, as it contributed to larger pore sizes while maintaining the nanopaper's density (Norrahma *et al.*, 2023). Consequently, the study indicates that NFC filter paper with suitable cellulose dosages can maintain high water permeability and structural integrity, making it a promising material for filtration applications requiring high permeability and robust rejection capacity.

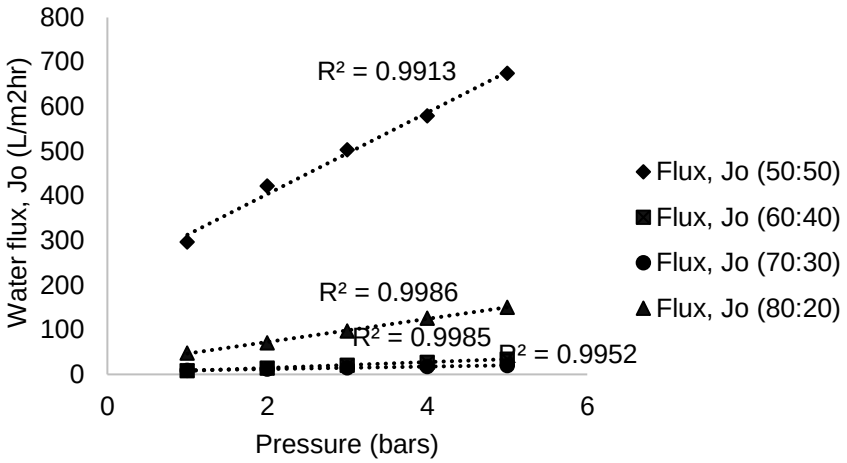

Figure 8 Distilled water flux vs pressure for different NFC filter paper cellulose dosages.

Blocking filtration mechanism of NFC filter paper

Membrane fouling is typically indicated by a notable increase in filtration resistance, which manifests as a significant rise in pressure over time when operating at a constant rate, or as a sharp reduction in flux over time when operating under constant pressure. This study examined two distinct stages of fouling mechanisms. In the first stage, there was a rapid initial flux decline, followed by a consistent decrease throughout the filtration period. The second stage was marked by a gradual decline in flux, eventually reaching a plateau and maintaining a steady rate until the filtration process concluded (Iritani & Katagiri, 2016; Norrahma *et al.*, 2023).

Table 1 summarizes the results of the blocking filtration laws applied to different dosages of NFC filter paper for treating synthetic dye solutions using a crossflow filtration system. The table includes the correlation coefficients (R^2) and the fitted parameter constant (K), highlighting the most appropriate model for each dosage. A higher R^2 value signifies a strong correlation, indicating that the chosen model accurately represents the fouling mechanism. The findings suggest that the blocking filtration laws effectively capture the compatibility and performance of NFC filter papers within the crossflow filtration system. Each dosage of NFC filter paper exhibited distinct fouling characteristics, which were well-explained by the models of complete blocking, intermediate blocking, standard blocking, and cake formation. These models not only help in understanding the fouling behaviour but also in predicting the filtration performance. The consistently high R^2 values across different dosages confirm the reliability of these models in identifying the dominant fouling mechanisms and their impact on filtration efficiency and membrane longevity.

Table 1: Prediction of fouling mechanism of different NFC filter paper to treat industrial textile wastewater effluent.

Blocking filtration mechanism	Stage		NFC filter paper			
			50:50	60:40	70:30	80:20
Complete blocking	1	R^2	0.9495	0.9015	0.1327	0.8527
	1	K (s^{-1})	<0.1	-0.0003	0.0002	-0.0002
	2	R^2	0.8803	0.0241	0.0726	0.9633
	2	K (s^{-1})	-0.0003	<0.1	<0.1	<0.1
Intermediate blocking	1	R^2	0.8820	0.9381	0.1561	0.8662
	1	K (s^{-1})	0.0009	0.0003	-0.0002	0.0002
	2	R^2	0.9437	0.0174	0.0739	0.9598
	2	K (s^{-1})	0.0018	<0.1	<0.1	0.0001

	1	R^2	0.9237	0.9219	0.1459	0.8603
Standard	1	K (s^{-1})	0.0003	0.0001	-0.001	0.0001
blocking	2	R^2	0.9179	0.0206	0.0733	0.9617
	2	K (s^{-1})	0.0003	<0.1	<0.1	<0.1
	1	R^2	0.7682	0.9579	0.1677	0.8733
Cake	1	K (s^{-1})	0.0029	0.0005	-0.0006	0.0006
formation	2	R^2	0.9648	0.0120	0.0749	0.9554
	2	K (s^{-1})	0.0276	<0.1	<0.1	0.0002

Additionally, Figure 9 illustrates the mechanism by which pollutants are removed using NFC filter paper, primarily governed by the size exclusion principle. The varying sizes of pollutant molecules in the wastewater sample play a crucial role in determining the effectiveness of the filtration. As the filtration progresses, the fibrous network of the NFC filter paper captures these molecules within its porous structure. The smaller molecules are initially trapped within the smaller pores, while larger molecules are retained on the surface or within the larger voids. Over time, as more pollutants are captured, the voids within the NFC filter paper become increasingly filled, leading to the gradual coverage of the filter paper's surface by contaminants (Norrahma *et al.*, 2023). This accumulation eventually results in the complete blockage of the filter, effectively preventing any further passage of pollutants and yielding a clean permeate solution. Although the NFC filter paper demonstrates high efficacy in removing dye molecules, the study identified fouling as a persistent challenge. The fouling issue arises from reduced net driving force across the filter paper, primarily due to the extensive and deep formation of a dye layer on the surface. This dye layer significantly increases flow resistance, reducing filtration efficiency over time.

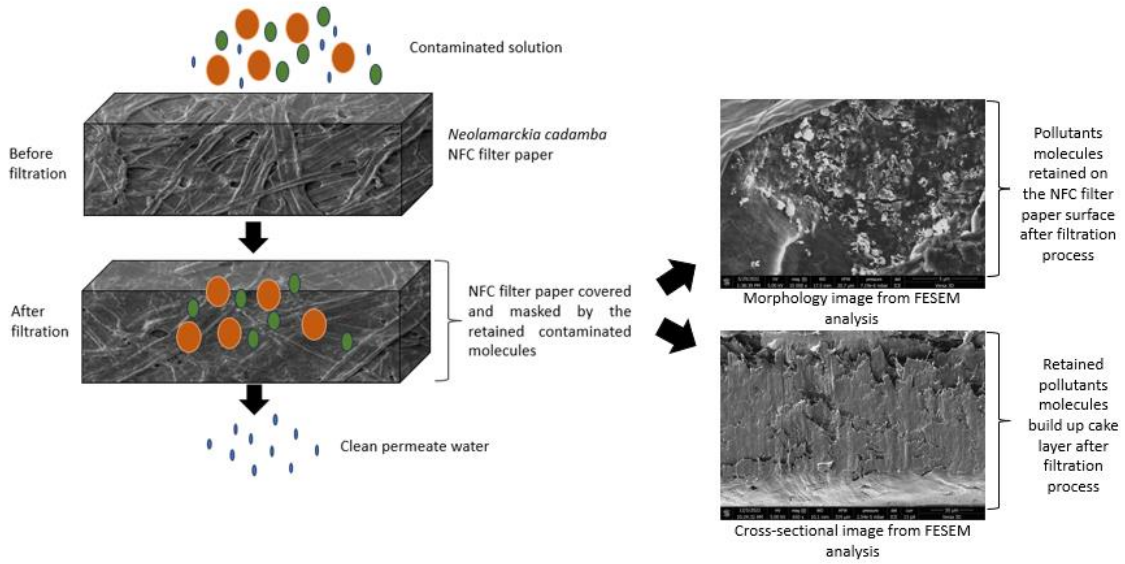

Figure 8 Mechanism of NFC filter paper in contaminated solution purification.

Furthermore, the fouling is exacerbated by the continuous deposition of pollutants, leading to a compact and dense layer that hinders the flow of the permeate (Sidik *et al.*, 2019). The decline in efficiency is not just a result of surface fouling but also due to the internal clogging of the pores within the NFC filter paper. As a result, the filtration process requires more pressure to maintain the same flux, leading to higher operational costs and potential damage to the filtration system over extended periods. This understanding underscores the importance of ongoing research into optimizing NFC filter paper design and developing effective fouling mitigation strategies to enhance the long-term performance and sustainability of filtration systems used in industrial textile wastewater treatment.

50:50 NFC filter paper

The analysis of the blocking mechanism began with the evaluation of the 50:50 dosage of NFC filter paper. It was determined that this dosage was not well-suited to the intermediate and standard blocking mechanisms, as indicated by R^2 values below 0.9, reflecting an insufficient correlation for both stages of the filtration process. In the initial phase, the filtration process was dominated by the complete blocking mechanism, as pollutants obstructed the entrance voids of the fibrous networks in the NFC filter paper, resulting in an R^2 value of 0.9495. Subsequently, as the filtration progressed to the second stage, a cake layer began to form and grow, evidenced by a higher R^2 value of 0.9648. The varying sizes of pollutant molecules likely influenced this transition in the textile wastewater, which led to pore blockage and hindered further penetration into the NFC filter paper.

The rapid formation of a dense gel layer in the later stage of filtration was attributed to the coagulation and deposition of differently-sized pollutant molecules on the surface of the NFC filter paper. This phenomenon, combined with the nano-scale dimensions of the cellulose fibre networks, contributed to the substantial resistance against the permeation of the textile wastewater through the filter. The decline in permeate flux further corroborated these findings, confirming that the primary fouling mechanisms for the 50:50 dosage combined blocked filtration and cake layer formation. These insights underscore the importance of understanding the interactions between pollutant size, filter structure, and fouling behaviour, which are crucial for optimizing filtration performance in textile wastewater treatment. This analysis also highlights the potential need for adjusting the NFC filter paper composition to better accommodate different fouling mechanisms and improve overall filtration efficiency.

60:40 NFC filter paper

Additionally, the results for the NFC filter paper with a 60:40 dosage revealed that at the initial stage of the filtration process, a cake layer formed on the filter paper surface due to the coagulation of textile wastewater pollutants. This layer effectively masked the surface of the NFC filter paper, as indicated by an R^2 value of 0.9579, suggesting a strong correlation with the cake formation model. However, as the filtration process continued into the second stage, the data showed a poor fit with the expected membrane fouling mechanisms, indicating an insignificant correlation. This discrepancy could be attributed to the prolonged operational time required for the crossflow filtration process.

The findings suggest that using a 60:40 NFC filter paper dosage may not be suitable for extended operational periods beyond 2 hours. A contributing factor could be the reduction of void spaces between the fibres in the NFC filter paper due to the higher concentration of nanofibrillated cellulose. This increased density likely restricted the passage of wastewater pollutants through the filter paper, limiting the permeate flow and potentially leading to inefficient filtration over time. This outcome highlights the need for optimization in the dosage of NFC and operational parameters to ensure effective and sustainable filtration, especially for extended treatment durations. It also underscores the importance of tailoring the filter paper composition to the specific requirements of the filtration process, particularly when dealing with complex wastewater streams like those from textile industries.

70:30 NFC filter paper

The 70:30 dosage of NFC filter paper also demonstrated unsatisfactory results, as none of the blocking mechanisms were found to be a good fit or significant during either stage of the filtration process. The tightly interwoven and narrow structure of the nanocellulose fibre networks likely contributed to increased resistance to permeate flow, making it difficult for the textile wastewater to penetrate the surface barrier of the NFC filter paper effectively. This elevated resistance impeded the filtration efficiency and suggests that the filter paper's structure may have been too dense for optimal performance in this application. The dense network of fibres may have caused excessive fouling and clogging, further hindered the passage of the wastewater and led to a decline in overall filtration effectiveness.

This finding underscores the need to carefully balance the composition and structural properties of NFC filter paper to achieve both adequate permeability and effective pollutant removal. Moreover, the poor fit of the blocking mechanisms at this dosage ratio indicates that the filtration dynamics may be

influenced by factors not fully accounted for by standard models, such as the complex interaction between the fibre networks and the diverse array of pollutants present in textile wastewater. This highlights the importance of further investigation and potential adjustments in the formulation of NFC filter papers to optimize their performance for specific filtration applications.

80:20 NFC filter paper

In contrast, the blocking behaviour observed with the 80:20 NFC filter paper dosage revealed that none of the blocking mechanisms provided a satisfactory fit during the initial filtration stage. This was evidenced by the coefficient of determination (R^2) values, which fell below the acceptable threshold of 0.9. The lack of a strong fit suggests that during this early stage, the filtration dynamics were not dominated by any single fouling mechanism, possibly due to the complex interactions and distribution of pollutants in the wastewater. However, a notable shift occurred as the filtration process progressed into the second stage. The formation of a gel or cake layer began to intensify, as indicated by a higher R^2 value of 0.9633, signalling that the fouling mechanism at this stage aligned more with the cake formation model. This aggressive build-up of the gel/cake layer can be attributed to the aggregation of varying-sized pollutant molecules, which led to significant coagulation and subsequent deposition at the surface of the NFC filter paper.

This condition caused a marked decrease in permeate flux, primarily because the increasing mass of retained pollutants formed a dense layer that further obstructed the flow through the filter paper. The growing layer of pollutants essentially masked the filter surface, creating a barrier that increased resistance and reduced the filtration efficiency. The significant fouling observed in the later stages highlights the importance of optimizing the dosage and structural properties of NFC filter paper to manage fouling and maintain consistent filtration performance over time. This observation underscores the complex nature of membrane fouling, particularly in systems treating heterogeneous mixtures such as textile wastewater, and the necessity for carefully tailored filtration strategies to mitigate these challenges.

Conclusion

This study utilized Weisner and Aptel's pore blocking models to analyze the fouling mechanisms in nanofibrillated cellulose (NFC) filter papers with varying dosage ratios during the treatment of industrial textile wastewater. The results indicated that each dosage ratio of NFC filter paper exhibited distinct blocking mechanisms at different stages of the 2-hour filtration process. The variation in blocking mechanisms was primarily influenced by the pollutant molecules' size and the voids within the nanofibrillated cellulose fibre networks. As the nanocellulose content in the filter paper increased, the formation of a cake layer became the predominant fouling mechanism, leading to a reduction in permeate flux over time. These findings underscore the critical importance of understanding and managing fouling mechanisms to optimize filtration processes. Specifically, the dominance of cake formation highlights the necessity for strategies that effectively control this type of fouling to maintain consistent filtration performance and efficiency in treating textile wastewater.

Acknowledgement

The authors would like to acknowledge Forest Research Institute Malaysia (FRIM) for providing the lab instrument for the preparation of CNF filter paper. The authors thank the Ministry of Education Malaysia for supporting this research under the Fundamental Research Grant Scheme (Code Grant: RACER/1/2019/TK10/UTHM//1 and partially sponsored by Universiti Tun Hussein Onn Malaysia.

References

Alsawaftah, N., Abuwatfa, W., Darwish, N., & Husseini, G. (2021). A comprehensive review on membrane fouling: Mathematical modelling, prediction, diagnosis, and mitigation. *Water (Switzerland)*, *13*(9). MDPI AG.

Amin, I. N. H. M., & Nizam, M. H. M. (2016). Assessment of membrane fouling indices during removal of reactive dye from batik wastewater. *Journal of Water Reuse and Desalination, 6*(4), 505–514.

Desa, A. L., Hairom, N. H. H., Ng, L. Y., Ng, C. Y., Ahmad, M. K., & Mohammad, A. W. (2019). Industrial textile wastewater treatment via membrane photocatalytic reactor (MPR) in the presence of ZnO-PEG nanoparticles and tight ultrafiltration. *Journal of Water Process Engineering, 31*.

Fernández, X. R., Rosenthal, I., Anlauf, H., & Nirschl, H. (2011). Experimental and analytical modeling of the filtration mechanisms of a paper stack candle filter. *Chemical Engineering Research and Design, 89*(12), 2776–2784.

Hairom, N. H. H., Mohammad, A. W., & Kadhum, A. A. H. (2015). Influence of zinc oxide nanoparticles in the nanofiltration of hazardous Congo red dyes. *Chemical Engineering Journal, 260*, 907–915.

Hermia, J. (1985). Blocking filtration: Application to non-Newtonian fluids. In A. Rushton (Ed.), *Mathematical models and design methods in solid-liquid separation* (pp. 83–89). Springer Netherlands.

Ho, C. C., & Zydney, A. L. (2000). A combined pore blockage and cake filtration model for protein fouling during microfiltration. *Journal of Colloid and Interface Science, 232*(2), 389–399.

Iritani, E., & Katagiri, N. (2016). Developments of blocking filtration model in membrane filtration. *KONA Powder and Particle Journal, 33*, 179–202. Hosokawa Powder Technology Foundation.

Latifah, J., Nurrul-Atika, M., Sharmiza, A., & Rushdan, I. (2020). Extraction of nanofibrillated cellulose from kelempayan (Neolamarckia cadamba) and its use as strength additive in papermaking. *Journal of Tropical Forest Science, 32*(2), 170–178.

Ma, Y., & Chew, J. W. (2022). Investigation of membrane fouling phenomenon using molecular dynamics simulations: A review. *Journal of Membrane Science, 661*. Elsevier B.V.

Marshall, A. D., Munro, P. A., & Trsgkdh, G. (1993). The effect of protein fouling in microfiltration and ultrafiltration on permeate flux, protein retention and selectivity: A literature review. *Desalination, 91*.

Nabi, M., Liang, H., Zhou, Q., Cao, J., & Gao, D. (2023). In-situ membrane fouling control and performance improvement by adding materials in anaerobic membrane bioreactor: A review. *Science of the Total Environment, 865*. Elsevier B.V.

Norrahma, S. S. A., Hamid, N. H. A., Hairom, N. H. H., Jasmani, L., & Sidik, D. A. B. (2023). Industrial textile wastewater treatment using Neolamarckia cadamba NFC filter paper via cross-flow filtration system. *Journal of Water Process Engineering, 55*.

Olaiya, N. G., Oyekanmi, A. A., Hanafiah, M. M., Olugbade, T. O., Adeyeri, M. K., & Olaiya, F. G. (2022). Enzyme-assisted extraction of nanocellulose from textile waste: A review on production technique and applications. *Bioresource Technology Reports, 19*.

Saeed, M. O., Azizli, K., Isa, M. H., & Bashir, M. J. K. (2015). Application of CCD in RSM to obtain optimize treatment of POME using Fenton oxidation process. *Journal of Water Process Engineering, 8*, e7–e16.

Samsami, S., Mohamadi, M., Sarrafzadeh, M. H., Rene, E. R., & Firoozbahr, M. (2020). Recent advances in the treatment of dye-containing wastewater from textile industries: Overview and perspectives. *Process Safety and Environmental Protection, 143*, 138–163.

Shen, M., Zhao, Y., Liu, S., Hu, T., Zheng, K., Wang, Y., Lian, J., & Meng, G. (2023). Recent advances on micro/nanoplastic pollution and membrane fouling during water treatment: A review. *Science of the Total Environment, 881*. Elsevier B.V.

Sidik, D. A. B., Hairom, N. H. H., Ahmad, M. K., Madon, R. H., & Mohammad, A. W. (2020). Performance of membrane photocatalytic reactor incorporated with ZnO-Cymbopogon citratus in treating palm oil mill secondary effluent. *Process Safety and Environmental Protection, 143*, 273–284.

Sidik, D. A. B., Hairom, N. H. H., & Mohammad, A. W. (2019). Performance and fouling assessment of different membrane types in a hybrid photocatalytic membrane reactor (PMR) for palm oil mill

secondary effluent (POMSE) treatment. *Process Safety and Environmental Protection, 130*, 265–274.

Tanudjaja, H. J., Anantharaman, A., Ng, A. Q. Q., Ma, Y., Tanis-Kanbur, M. B., Zydney, A. L., & Chew, J. W. (2022). A review of membrane fouling by proteins in ultrafiltration and microfiltration. *Journal of Water Process Engineering, 50*. Elsevier Ltd.

Yousefi, N., Jones, M., Bismarck, A., & Mautner, A. (2021). Fungal chitin-glucan nanopapers with heavy metal adsorption properties for ultrafiltration of organic solvents and water. *Carbohydrate Polymers, 253*.